BMC Medical Imaging

RESEARCH

Open Access

Comprehensive assessment of imaging quality of artificial intelligence-assisted compressed sensing-based MR images in routine clinical settings

Adiraju Karthik[1], Kamal Aggarwal[2], Aakaar Kapoor[3], Dharmesh Singh[4*], Lingzhi Hu[5], Akash Gandhamal[4] and Dileep Kumar[4]

Abstract

Background Conventional MR acceleration techniques, such as compressed sensing, parallel imaging, and half Fourier often face limitations, including noise amplification, reduced signal-to-noise ratio (SNR) and increased susceptibility to artifacts, which can compromise image quality, especially in high-speed acquisitions. Artificial intelligence (AI)-assisted compressed sensing (ACS) has emerged as a novel approach that combines the conventional techniques with advanced AI algorithms. The objective of this study was to examine the imaging quality of the ACS approach by qualitative and quantitative analysis for brain, spine, kidney, liver, and knee MR imaging, as well as compare the performance of this method with conventional (non-ACS) MR imaging.

Methods This study included 50 subjects. Three radiologists independently assessed the quality of MR images based on artefacts, image sharpness, overall image quality and diagnostic efficacy. SNR, contrast-to-noise ratio (CNR), edge content (EC), enhancement measure (EME), scanning time were used for quantitative evaluation. The Cohen's kappa correlation coefficient (*k*) was employed to measure radiologists' inter-observer agreement, and the Mann Whitney U-test used for comparison between non-ACS and ACS.

Results The qualitative analysis of three radiologists demonstrated that ACS images showed superior clinical information than non-ACS images with a mean *k* of ~ 0.70. The images acquired with ACS approach showed statistically higher values ($p < 0.05$) for SNR, CNR, EC, and EME compared to the non-ACS images. Furthermore, the study's findings indicated that ACS-enabled images reduced scan time by more than 50% while maintaining high imaging quality.

Conclusion Integrating ACS technology into routine clinical settings has the potential to speed up image acquisition, improve image quality, and enhance diagnostic procedures and patient throughput.

Keywords Artificial intelligence assisted compressed sensing, Magnetic resonance imaging, Qualitative analysis, Quantitative analysis, Scan duration

*Correspondence:
Dharmesh Singh
dharmeshsingh03@gmail.com
Full list of author information is available at the end of the article

Introduction

Magnetic Resonance Imaging (MRI) is an important medical imaging tool that can generate high-resolution, multi-parametric, and multi-directional anatomical images, making it an essential tool in the diagnosis and prognosis monitoring for different diseases [1]. In recent years, a significant amount of work has been done to improve MRI sequences in terms of their field of view, resolution, and acquisition duration. The longer duration of an MRI examination is often mentioned as one of the key challenges of the diagnostic process for both patients and radiology departments which can lead to motion artifacts and distort the image quality for accurate diagnosis [2, 3]. This can be particularly challenging for patients who may have difficulty in holding breath for long time during scans. Additionally, longer scanning times significantly increase healthcare costs and accessibility, especially in nations with a lack of MR scanners [4]. Therefore, the requirement of fast MR scans in clinical settings is essential. In clinical practice, reducing scan acquisition time increases patient throughput, enhances scanner efficiency, improves image quality, promotes better patient compliance, and minimizes motion artifacts [5, 6].

The MR imaging cycle is repeated multiple times with the total number of repetitions depending on the image quality desired during the acquisition process. Signal-to-noise ratio (SNR) and contrast-to-noise ratio (CNR) are important scanner performance parameters that are utilized in MRI for quality assurance [7]. Most clinical applications require an appropriate trade-off between scan time and spatial resolution. It has been observed that the edge content, brightness, and contrast of an image play an important role in the development of computer-aided diagnosis systems [8]. All these factors are taken into consideration during quantitative measurements such as segmentation, classification and morphological change analysis [9].

As clinical examinations become more prevalent, novel accelerated imaging technologies are essential for enabling ultra-fast scanning while producing high-quality images [10]. Various imaging acceleration techniques, such as compressed sensing (CS), parallel imaging (PI), and half Fourier (HF) acquisition were devised to address the issue of longer scanning times [11, 12]. In recent times, CS-based techniques which is a nonlinear mathematical model that successfully suppresses noise bands and acceleration-induced artefacts have been developed and employed in several clinical studies [4, 13]. These methods for image acceleration speed up imaging but degrade image quality. The limitations of traditional MR acceleration techniques are as follows: CS can struggle with noise and artifacts; PI often encounters reduced SNR and artifacts, especially at higher acceleration factors and HF can cause blurring and increased susceptibility to artifacts due to incomplete k-space data. The widespread use of deep learning (DL) model, such as convolutional neural networks (CNNs), combined with standard acceleration technologies has demonstrated significant potential in accelerated MRI, as artificial intelligence (AI) becomes increasingly prevalent.

In the past, DL/AI has shown immense promise across multiple domains, including drug discovery [14, 15], medical image analysis [16–21], and signal processing [20, 21], establishing itself as a valuable tool in advancing healthcare technologies. Specifically, machine learning (ML) models have been used to predict drug permeability across the placenta [14] and to redirect drugs to the blood–brain barrier using advanced fingerprint amalgamation and data balancing techniques [15]. In medical image analysis, DL/AI approaches have greatly enhanced image segmentation, lesion detection, and image quality improvement. For example, AI techniques have played a crucial role in breast cancer assessment through elastography ultrasound [16] and have demonstrated promising outcomes in ultrasound segmentation [17, 18] and liver CT segmentation using lightweight neural networks [19]. Additionally, AI has significantly advanced signal processing applications, such as analysing electrocardiogram (ECG) signals to provide deeper insights into signal interpretation [20, 21].

AI-assisted compressed sensing (ACS) is an advanced MR acceleration solution that integrates multiple technologies to improve MRI speed and quality, enabling more efficient imaging without compromising diagnostic accuracy. ACS combines the CS, PI, HF, and CNN to overcome the limitations of traditional acceleration techniques [13, 22]. The ACS has shown the potential in a few applications, including imaging of the liver [13, 23], knee [24], and kidney [25]. A recent systematic review by Priyanka et al. [26] evaluated the impact of ACS technique on scan time and image quality in musculoskeletal MRI. The review concluded that ACS effectively reduces scan time while enhancing image quality for both 2D and 3D MSK-MRI sequences compared to PI and CS. Although previous studies have compared various ACS approaches with conventional MR imaging techniques, there remain important gaps in the literature. Most prior research has focused on specific anatomical regions, limiting their generalizability across different body areas. Furthermore, many studies have been conducted in controlled research settings, which do not fully reflect the challenges encountered in routine clinical practice. This current study aims to address these gaps by providing a comprehensive, real-world assessment of ACS across multiple anatomies such as brain, spine, liver, kidney and knee. The objective of

this study was to evaluate the image quality of the ACS technique across multiple body regions, including the brain, spine, liver, kidney, and knee, using both qualitative and quantitative analyses, while also examining the effect of ACS on scan time.

Methods

MRI data acquisition

In this study, 50 subjects (mean age: 44 years, age range: 25 to 67 years) were randomly selected to undergo MR examination of different body regions such as brain, spine, kidney, liver, and knee prospectively. Ten MR datasets acquired for each body region with and without ACS technique using different MR contrasts. All MR scans were acquired using a 3T MR scanner (uMR 780, United Imaging Healthcare Co. Ltd, Shanghai, China) at Sprint Diagnostics, Hyderabad, India from September 2022 to February 2023 with the prior approval from the Institutional Review Board (IRB), committee (ref:S-2022001) of Sprint Diagnostics, Hyderabad. Before the examination, informed consent was obtained from all subjects and/or their legal guardian(s). This study was performed in accordance with institute guidelines and regulations. The inclusion criteria for the participants' selection were as follows: a) healthy subjects with no known medical history, b) adults aged 18–70 years, c) who are able to provide written informed consent as well as who can adhere to the study protocols. The exclusion criteria were: (a) any known neurological, abdominal, impaired renal function, spine disease or musculoskeletal conditions that could potentially affect with the imaging results, (b) those whose image quality cannot meet the diagnostic requirements. c) contraindications to MRI, such as claustrophobia or incompatible implants.

A dedicated 24-channel head-neck coil was used for brain MR scanning, and a 32-channel spine coil was employed for spine exams. A dedicated 12-channel coil was employed for knee MR, and a combination of a 12-channel body coil and a 12-channel spine coil was used for the liver and kidney. Table 1 presents a comprehensive overview of the contrast and protocol parameters used in this study.

ACS image reconstruction

The FDA-approved ACS technique uses CNN to accelerate image acquisition. The ACS reconstruction network utilizes a generative adversarial architecture comprising a generator and a discriminator. The discriminator, implemented as a CNN, differentiates between real and generated images by classifying them as either authentic or reconstructed, thereby encouraging the generator to create images that closely resemble fully sampled versions.

Table 1 Scanning protocols of all sequences

Sequences	Non-ACS				ACS			
	TR	TE	AM	AD	TR	TE	AM	AD
Brain								
T1W FSE Flair TRA	2023	22.96	334×384	02:01	2023	22.96	334×384	00:53
T2W FSE Flair with FS TRA	9000	103.32	300×384	02:24	9000	103.32	300×384	01:30
T1W FSE TRA	375	6.32	528×459	02:08	375	6.32	528×459	00:57
T2W FSE TRA	5552	118.08	417×480	01:07	5552	118.08	417×480	00:39
Spine								
T2W FSE SAG C SPINE	5421	113	600×685	02:21	5421	113	600×685	01:00
T2W FSE SAG L SPINE	2801	121	600×750	03:14	2801	121	600×750	03:05
T2W FSE SAG T SPINE	4000	121	600×685	01:44	4000	121	600×685	00:44
T1W FSE Sag	550	8.16	384×576	01:49	550	8.16	384×576	00:51
Liver								
T2W_NAVI (Non-ACS) and T2W FSE with FS and BH (ACS)	2775	85	672×530	03:53	2775	85	672×530	01:85
Kidney								
T2W_NAVI (Non-ACS) and T2W FSE with FS and BH (ACS)	2775	85	672×530	04:13	2775	85	672×530	01:90
Knee								
PD FSE COR FS	2780	38.30	456×456	03:34	2780	38.30	456×456	01:54
T2 FSE SAG	3200	118	576×576	04:10	3200	118	576×576	01:49
T1W FSE TRA	686	8	600×600	04:13	686	8	600×600	01:47

TR Repetition time (ms), *TE* Echo time (ms), *AM* Acquisition matrix, *AD* Acquisition duration, *T1W* T1-weighted, *T2W* T2-weighted, *FSE* Fast spin echo, *TRA* Transverse, *FS* Fat saturation, *SAG* Sagittal, *BH* Breath hold, *COR* Coronal, *NAVI* Navigator, *PD* Proton density

To reduce uncertainty, ACS integrates the trained AI module's output as a constraint in the CS framework, incorporating a regularization factor based on the difference between the reconstructed image and the AI module's predicted image, as described in the previous study [27]. The ACS network solves an optimization problem where the objective was to minimize the reconstruction error between the undersampled k-space data and the fully reconstructed image. The data fidelity term ensures that the reconstructed image remains consistent with the acquired undersampled data, while regularization constraint suppresses noise and enhance image quality. The general equation for the optimization is:

$$\widehat{x} = \arg\min_{x} \left\{ \|Fu(x) - y\|_2^2 + \lambda R(x) + \alpha\, C(x,\theta) \right\} \tag{1}$$

where $\widehat{x}$ is the reconstructed MRI image, Fu is the undersampled Fourier transform, y is the undersampled k-space data, $\|Fu(x) - y\|_2^2$ is the data fidelity term ensuring consistency with the acquired data, $R(x)$ is a regularization term to enforce smoothness and remove noise, λ is a regularization parameter balancing fidelity and regularization, $C(x,\theta)$ is the AI-based term that incorporates learned priors from a deep neural network. The AI model with parameters θ learns how to improve the image reconstruction based on training data.

The generator was based on the U-Net architecture, which is well-suited for image-to-image translation tasks, utilizing encoder and decoder blocks with skip connections to preserve spatial information during reconstruction. The network used in this study is similar to U-Net but includes a residual block with two convolution operations and a skip connection, replacing the conventional convolution operation in the original U-Net design. To further improve the quality of the reconstructed images, a least-squares generative adversarial network training technique was used [28, 29]. This technology has previously been used in single-breath-hold T2WI liver MRI [13], and the same network layout of the deep learning-based fast MRI reconstruction framework was used in the current study.

ACS reconstruction pipeline integrates a generative neural network, which is designed to infer missing k-space information and reconstruct high-quality MR images from undersampled data. The input to the network is undersampled k-space data, which is first zero-filled and passed through a series of encoding layers to capture low-level and global features of the image. The generative component of the network, crucial for image synthesis, utilizes these learned features to predict the missing k-space data, ensuring that the output remains anatomically accurate and free from artifacts. The final reconstructed image is produced by decoding these features back into image space, with the help of skip connections that preserve high-frequency details.

ACS uses a randomized undersampling pattern, providing 9 levels of undersampling in total. The corresponding acceleration factor varies from 2 to 4. Figure 1a displays the deep learning network structure, while Fig. 1b represents the ACS reconstruction pipeline.

Non-ACS reference approach

The non-ACS reference approach entails obtaining full k-space data without undersampling, enabling the inclusion of all data points. The reconstruction of the full sampling acquisition was carried out using a conventional method based on Fourier transform. This approach has been considered the gold standard for evaluating ACS-reconstructed images in this study.

Data processing

Qualitative evaluation

Following the MRI scan, images were transferred to an on-site Picture Archiving and Communication System system and uWS workstation (United Imaging Healthcare Co. Ltd., Shanghai, China) for clinical use. A standard scoring system was developed to assess the quality of images in terms of artefacts in the images, sharpness of tissue edges, overall quality of the images, and the diagnostic efficacy of the images. According to the criteria, the scores were assigned on a 5-point Likert scale ranging from 1 to 5. The detailed criteria for qualitative scoring are listed in Table 2. In this study, three radiologists (one with 5 years of experience and one with 20 years of experience with knowledge of the United Imaging Healthcare MR scanner and one radiologist with 5 years of experience but no knowledge of the United Imaging Healthcare MR scanner) were assessed all images independently and assigned scorers based on the following criteria (presented in Table 2).

Quantitative evaluation

The MR images were anonymized and transferred to a workstation following the radiologist's assessment of qualitative scores. The quantitative assessment was performed by calculating the SNR, CNR, edge content (EC), and enhancement measure (EME) for each image of all body regions. With the assistance of expert radiologists, three regions of interest (ROIs) were drawn at various tissue locations to obtain average signal intensities and standard deviation, as shown in Fig. 2. Figure 2 additionally included the selection criteria for ROI marking for brain, spine, liver, kidney, and knee images. Similar ROIs were used across

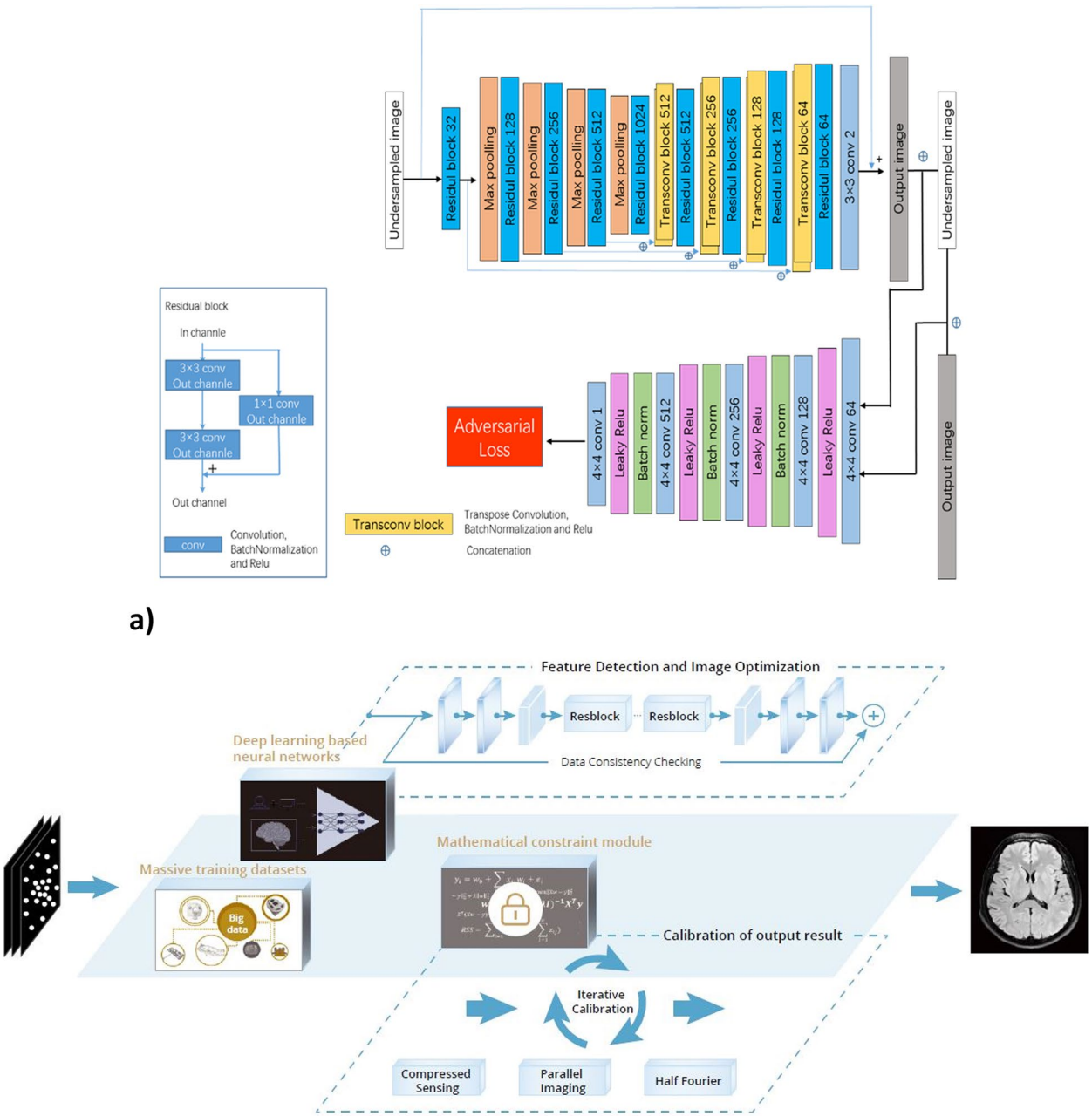

Fig. 1 **a** Deep learning network for fast MRI reconstruction framework used in this study (adopted from Sheng et al. (2021) [13]), **b** ACS reconstruction pipeline. ACS integrates specialized mathematical constraints with AI to achieve reliable results. The ACS module effectively remedies reconstruction errors in Parallel Imaging and Half Fourier method, while the reliability issues associated with deep learning's "black box" effect are solved by the mathematical iterative model which includes Compressed Sensing, phase constraints and data fidelity

all non-ACS and ACS datasets from the same subject. The SNR, CNR, EC and EME measurements were carried out using the in-house routines of MATLAB (v.2018; MathWorks). Scanning time was also incorporated to the study as a quantitative parameter to demonstrate the capabilities of ACS assisted imaging. The following quantitative metrics are calculated to evaluate image quality

1. SNR is defined as the ratio of the mean signal intensities of different ROIs to the standard deviation of the noise.

Table 2 Detailed scoring criteria for qualitative analysis

Parameter	Score	Descriptions
Image artifacts	**1**	Severe artifacts that obscure the majority of the image, significantly compromising diagnostic quality
	2	Moderate artifacts present, partially obscuring important anatomical structures and affecting diagnostic quality
	3	Minor artifacts present, which do not significantly obscure anatomical structures or compromise diagnostic quality
	4	Very minor artifacts, barely noticeable, and do not affect diagnostic quality
	5	No visible artifacts. The image is clear and free of any distortions
Overall image quality	**1**	Very poor quality. The image is non-diagnostic, and anatomical structures are not distinguishable
	2	Poor quality. The image is diagnostically useful but with significant limitations, and many anatomical structures are difficult to interpret
	3	Adequate quality. The image is diagnostically acceptable but with some limitations, and most anatomical structures are interpretable
	4	Good quality. The image is diagnostically useful with minor limitations, and all major anatomical structures are clear
	5	Excellent quality. The image is of high diagnostic value with no limitations, and all anatomical structures are clearly visible
Image sharpness	**1**	All edges are significantly blurred. Anatomical structures are difficult to distinguish, and fine details are completely lost
	2	Most edges are moderately blurred. Some anatomical structures are distinguishable, but fine details remain unclear
	3	Edges are slightly blurred. Most anatomical structures are distinguishable, but some fine details are only moderately clear
	4	Edges are mostly sharp. Anatomical structures are clear, and fine details are mostly preserved
	5	All edges are very sharp. Anatomical structures and fine details are clearly visible and well-preserved
Diagnostic efficiency	**1**	Non-diagnostic. The image cannot be used for clinical evaluation due to poor quality
	2	Suboptimal diagnostic efficiency. The image can be used for clinical evaluation but with significant difficulty and limitations
	3	Adequate diagnostic efficiency. The image is clinically useful but requires additional effort to interpret due to some limitations
	4	Good diagnostic efficiency. The image is clinically useful with only minor limitations, allowing for accurate interpretation
	5	Excellent diagnostic efficiency. The image is clinically very useful with no limitations, enabling straightforward and accurate interpretation

$$SNR = \frac{Mean\ of\ signal\ intensities}{Standard\ deviation\ of\ noise} = \frac{\underset{r=1..n}{mean} S(r)}{\underset{r=1..n}{stddev} N(r)} \tag{2}$$

2. CNR is defined as the difference in mean signal intensity ROIs divided by the standard deviation of the background noise.

$$CNR = \frac{Difference\ in\ signal\ intensities}{Standard\ deviation\ of\ noise} = \frac{\underset{r=1..n}{diff} S(r)}{\underset{r=1..n}{stddev} N(r)} \tag{3}$$

3. EC is commonly determined by computing the gradient magnitude of the image, which emphasizes regions with significant variations in intensity, which indicates the presence of edges [9, 30]. A Gaussian filter is applied to the image to reduce the impact of noise before calculating the gradient for EC. Thus, EC is given as follows,

$$EC = \frac{1}{A \times B} \sum_s \sum_t |G(s,t)| \tag{4}$$

where $A \times B$ is the size of the image and $1 \le s \le A$ and $1 \le t \le B$ and

$$|G| = \sqrt{G_s^2 + G_t^2} \tag{4.1}$$

where G is the gradient vector of image I given as

$$G(s,t) = \begin{bmatrix} G_s \\ G_t \end{bmatrix} = \begin{bmatrix} \frac{\partial}{\partial s} I(s,t) \\ \frac{\partial}{\partial t} I(s,t) \end{bmatrix} \tag{4.2}$$

4. EME is an image quality metric that evaluates the visibility of fine details and the level of contrast in an image [9, 31]. It is calculated as the average ratio of

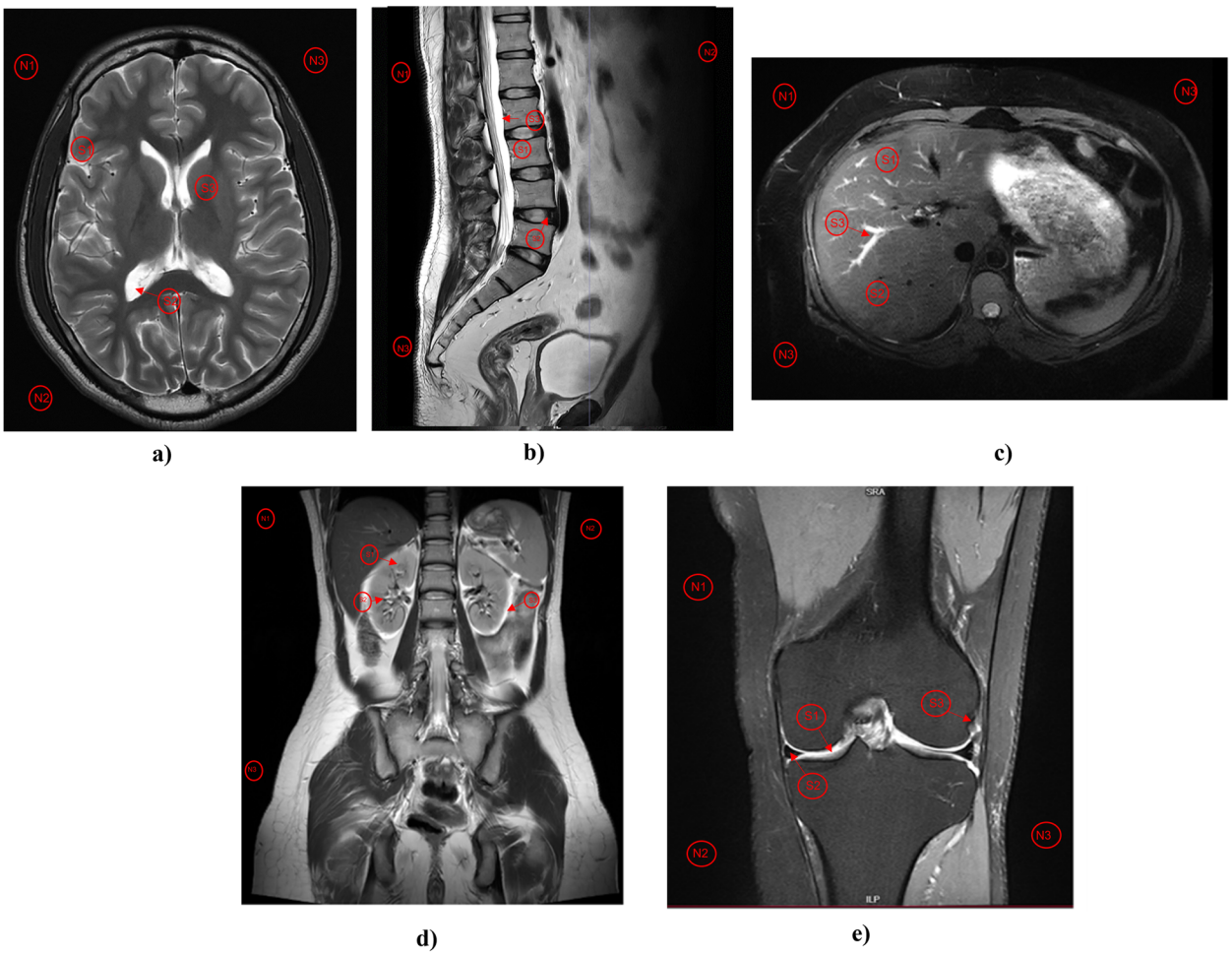

Fig. 2 ROI marking for quantitative evaluation for **a** brain: ROIs in the T2 FSE axial image of the brain are marked for detailed examination: S1 targets the gray matter near the caudate nucleus to identify any abnormalities, important for diagnosing neurodegenerative conditions. S2 focuses on the lateral ventricle to detect any changes in size or shape, significant for identifying hydrocephalus or other cerebrospinal fluid-related conditions. S3 is targeted in the white matter to look out for any abnormal myelination in the brain and serve as markers for small vessel disease. **b** spine: The ROIs in the lumbar spine T1W FSE ACS sagittal image are clinically significant areas marked to identify potential specific pathological changes: S1 highlights L3 disc to assess any degeneration, S2 assesses the nucleus polposus of the intervertebral discs for prolapse or bulges that may lead to radiating pain and sensitive changes that encompass nerve distribution, and S3 examines potential spinal cord compression in any affected area. **c** liver: ROIs in the liver T2W axial image are clinically significant areas marked to facilitate a comprehensive diagnostic evaluation. S1 focuses on the right hepatic artery to identify probable perfusion abnormalities, obstructions, stones, or dilations, which are critical for assessing vascular health and liver function. S2 and S3 are specifically marked on liver lobes IVa/b and VII/VI, respectively, to examine the liver parenchyma for signs of hemangiomas, which are common benign liver tumors, **d** kidney: ROIs in the kidney T2W coronal image are clinically significant areas marked for specific evaluations: S1 targets in the right kidney cortex to identify any pathological changes. S2 focuses on the minor calyx, clinically significant for detecting obstructions or infections affecting urine drainage. S3 examines perinephric fat, crucial for assessing inflammatory conditions or masses that can impact kidney function and surrounding structures., and **e** knee: ROIs in the PD FSE coronal image of the knee are clinically significant areas marked for the following purposes: S1 targets the articular cartilage in the middle compartment to assess for degeneration or damage, crucial for joint health. S2 focuses on the medial meniscus, identifying any tear or degeneration that can affect knee stability. S3 focuses on the lateral collateral ligament to look out for any potential tear or damage to the cartilage. image; S1/S2/S3 = Signal ROIs and N1/N2/N3 = Noise ROIs. ROI = Region of interest

the maximum ($I_{\max}$) to minimum pixel ($I_{\min}$) intensity within non-overlapping sub-blocks ($t_1 t_2$) of the image, which provides a measure of local contrast and detail visibility. The EME can be calculated using following equation:

$$\mathrm{EME} = \frac{1}{t_1 t_2} \Sigma_{j=1}^{t_2} \Sigma_{i=1}^{t_1} 20 \, log \frac{I_{max}}{I_{min}} \tag{5}$$

These parameters values were acquired from all sequences for 50 subjects and used to conduct statistical analysis.

Statistical analysis

All the statistical analysis was done in MedCalc, version 19.3 (MedCalc Software Ltd) software. The Mann–Whitney U-test and paired *t*-test were used to determine the statistical significance of the differences between qualitative and quantitative evaluations. The Cohen's kappa correlation coefficient (*k*) and bar graphs were used to show the inter-observer agreements of image quality between three radiologists for non-ACS and ACS images. Boxplots were also utilized to compare the quantitative parameters of non-ACS images with ACS images.

Results

Figure 3 shows the example of MR images acquired with and without the ACS technique for different body regions. Figure 3 provides a detailed description of the locations that illustrate the differences between non-ACS and ACS images across multiple sequences of brain, spine, liver, kidney, and knee imaging.

Qualitative evaluation

In this study, three radiologists independently assessed the non-ACS and ACS images for all 50 subjects using the proposed qualitative scoring criteria. A total of 532 non-ACS and ACS images, comprising 266 images in each group, were assessed and scored by each radiologist. All images were randomized before being presented to the radiologist for evaluation as well as all images were anonymized and labelled with a neutral identifier that does not indicate the acquisition technique. The radiologists evaluated the image quality of images based on multiple factors, including the presence of artefacts, level of sharpness, overall image quality, and diagnostic efficiency. The qualitative examination of three radiologists showed that the overall diagnostics quality and clinical information of images acquired with ACS were comparable or superior to images acquired without ACS. The Mann–Whitney U-test was performed separately for each anatomical region, showing no significant difference ($p > 0.05$) in qualitative scores between non-ACS and ACS across each region.

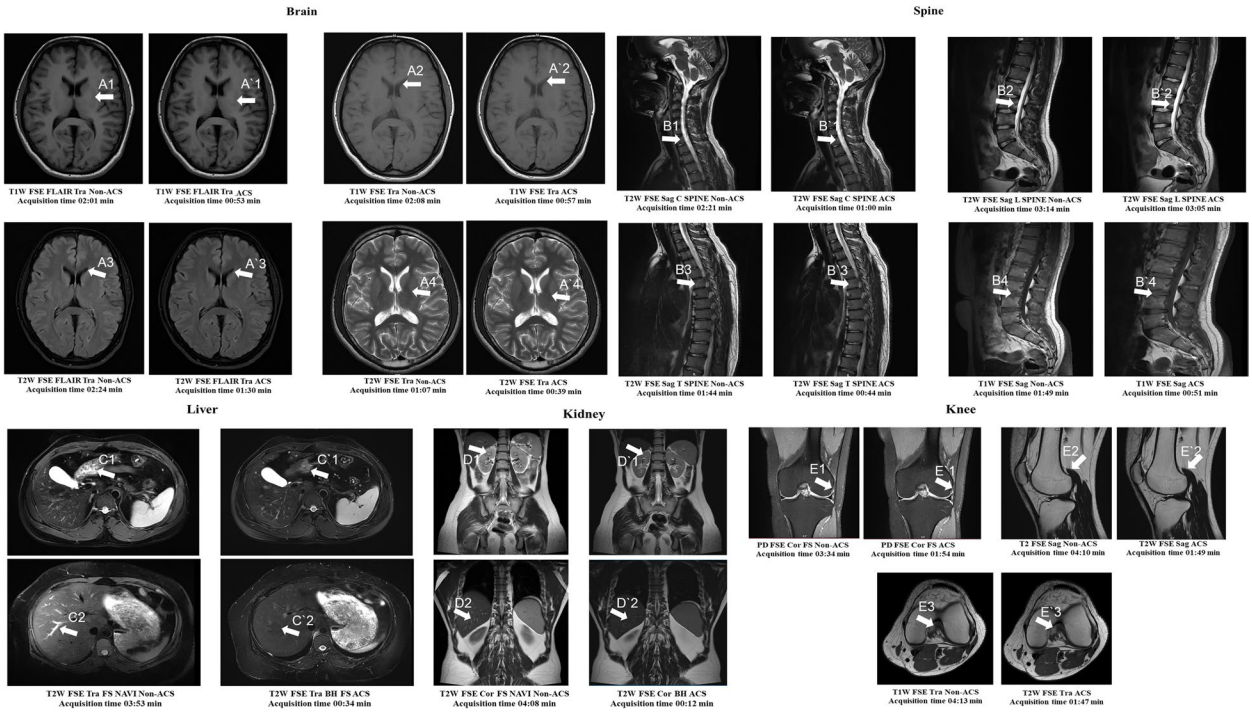

Fig. 3 Example of MR images of brain, spine, liver, kidney and knee regions acquired with and without the ACS technique. Arrows A showcases T1W and T2W axial brain images. The arrows point to the boundaries of anatomical structures: thalamus (A1, A`1), lateral ventricles (A2, A`2, A3, A`3), and putamen (A4, A`4). The ACS images (A`1, A`2, A`3, A`4) provide more distinct and clearer structural boundaries than the non-ACS images. Arrows B displays T2W FSE sagittal spine images. In B1/B`1, the distinct features of the vertebral body in the C7 cervical spine appears much clearer in B`1. B2/B`2 highlights vertebral body of the L3 spine looking out for any clinically significant pathology, with B`2 offering more details. B3/B`3 reveals the vertebral body of the thoracic spine, with B`3 showing enhanced features. B4/B`4 focuses on the nucleus polposus of the intervertebral disc, again with the ACS image (B`4) exhibiting better detailed features. Arrows C and D compare liver and kidney images respectively. indicating that ACS images exhibit superior fluid suppression, leading to better diagnostic clarity compared to non-ACS images (C and D). Section E depicts knee images. E1/E`1 shows lateral collateral ligament, with E`1 providing clearer details. Similarly, E2/E`2 and E3/E`3 demonstrate knee anatomical structures in sagittal and axial views, respectively, with ACS images offering superior quality and distinct detail

Furthermore, we conducted this test on all 532 images for overall comparison between the two sets of images, However, no significant difference was found between them. There was a good kappa coefficient ($k = 0.65–0.70$) between all radiologist assessment. Figure 4 shows bar plots for comparison of non-ACS and ACS images based on qualitative assessment by three radiologists.

Quantitative evaluation

All quantitative parameters were measured from each sequence obtained with and without ACS. Mean ± standard deviation values of SNR, CNR, EC and EME across all sequences were 41.20 ± 2.49, 23.93 ± 3.35, 31.58 ± 23.08, and 9.36 ± 1.56 for images acquired without ACS whereas the mean values for ACS images were 43.91 ± 2.10, 26.38 ± 3.76, 41.43 ± 27.39, and 13.52 ± 3.83, respectively. Table 3 illustrates the quantitative parameter values across each region.

All quantitative parameters values were found to be higher in images acquired with ACS than in images acquired without ACS in five body regions. According to the paired *t*-test, ACS-based measurements showed substantially higher values ($p < 0.05$) for both SNR and CNR as compared to non-ACS measurements.

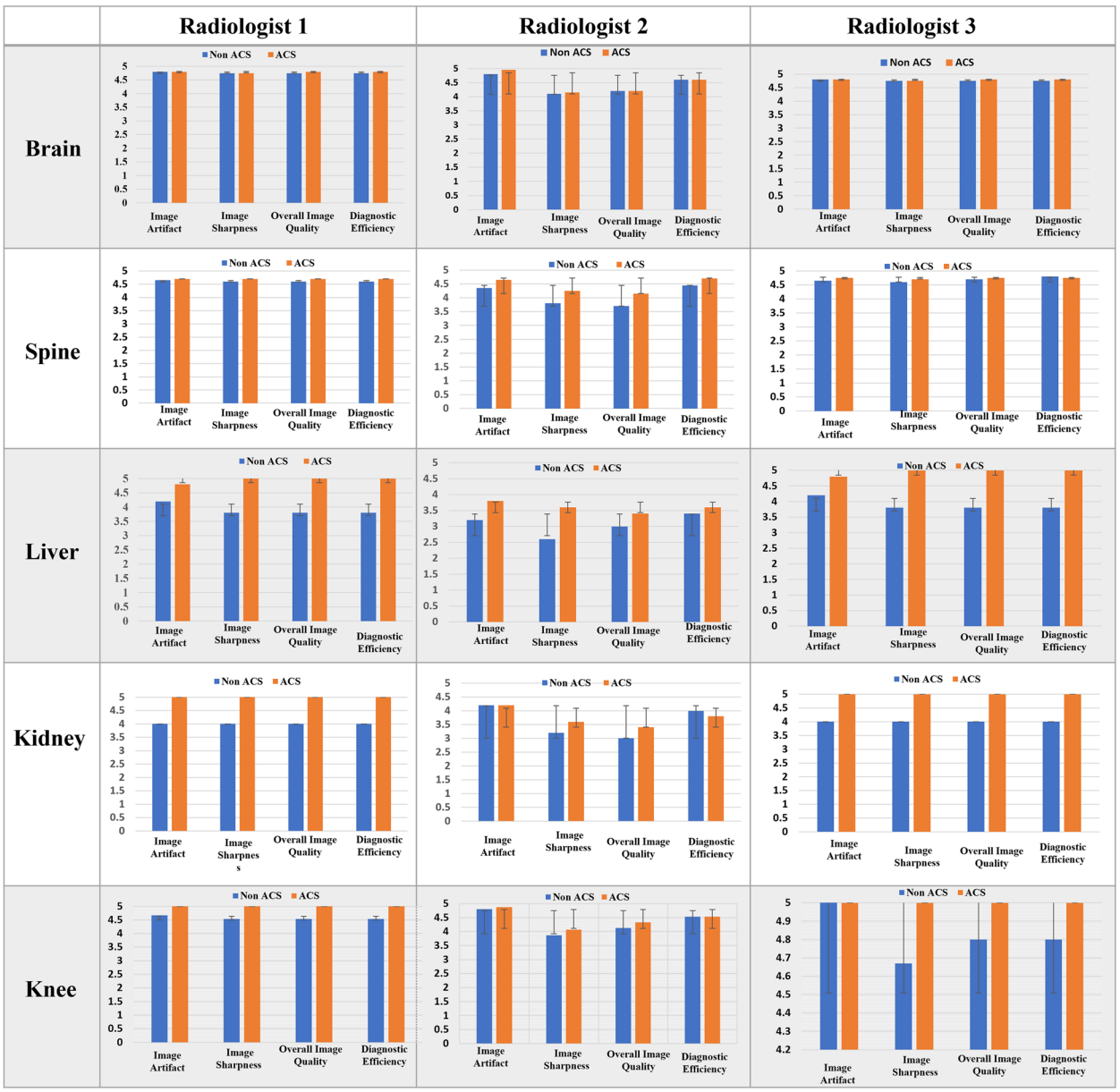

Fig. 4 Bar plots comparing non-ACS versus ACS images based on three radiologists' qualitative evaluations

Figures 5 and 6 show the boxplots distribution of SNR, CNR, EC and EME values for non-ACS and ACS images of different body regions.

Total scanning time for all sequences obtained in each body region was determined to compare differences in scan duration. For an example, T1-weighted FSE, T2-weighted FSE, T1-weighted FSE Flair, T2-weighted FSE Flair with FS were acquired in brain region with and without ACS technique and the total time was calculated for all 4 sequences acquired with ACS and without ACS. Similarly, the total scanning duration for each of the five body regions included in this study was determined. Figure 7 shows the total scanning time across each body regions. The differences in scanning time of ACS enabled sequences as compared to non-ACS sequences shows significant improvements in scanning time of ACS enabled sequences. Scan times were reduced by 48.10%, 55.52%, 52.44%, 54%, and 50% for brain, spine, liver, kidney, and knee ACS exams, respectively, while maintaining better and comparable quality of images with routine acquisitions. A comparison of the reconstruction times with similar protocols showed no significant difference between the reconstruction times of ACS and non-ACS. Reconstruction time of non-ACS was only 1–2 s faster than ACS. ACS showed comparable subjective image quality in the comparison of non-ACS, with the added benefit of significantly reduced scan times, making it especially useful in time-sensitive clinical settings.

Discussion

Magnetic Resonance Imaging is a safe and effective imaging method that provides exceptional soft tissue resolution. The presence of motion artifacts during MRI scans requires repeated scans, leading in an estimated additional cost of $115,000 per device per year. In the United States alone, this leads to an annual expenditure of over $1.4 billion, as repeat MRI sequences are required for 19.8% of patients [32]. One of the main reasons for this is because patients feel uncomfortable or in pain throughout the quite long MRI scan, hence accelerating the scan is essential [32]. The ratio of acceleration level, image quality, and scan time significantly impacts the overall effectiveness and feasibility of the diagnosis in MRI.

However, one limitation of CS is the challenges involved in determining the optimal level of sparseness for applications. This usually requires tuning the hyperparameters manually which is time consuming and difficult to standardize [33, 34]. Recent improvements in AI algorithms that allow for faster imaging overcome the shortcomings of CS. Hammernik et al. [34] and Knoll et al. [35] proposed a "variational" network that was based on CNN. This network was essentially an extension of PI and CS that was used for deep learning, and it successfully reconstructed accelerated knee images [34, 35]. The AI based compressed sensing technique has been previously shown potential in a few clinical applications such as liver imaging [13, 23], knee imaging [24] and kidney imaging [25]. A recent systematic review by Priyanka et al. [26] showed a significant reduction in scan time and improved image quality for 2D and 3D sequences in musculoskeletal MRI compared with PI and CS.

The conventional (non-ACS) reference approach involves acquiring full k-space data without undersampling and reconstructing the full sample acquisition using a traditional method based on the Fourier transform. In this study, T1W FSE FLAIR, T2W FSE FLAIR with FS, T1W FSE and T2W FSE sequences for brain imaging; T2W FSE SAG and T1W FSE sequences for spine imaging; T2W NAVI and T2W FSE with FSE and BH for liver and kidney imaging; and PD FSE, T2W FSE and T1W FSE sequences for knee imaging showed the benefit in terms of imaging quality and acquisition time from the novel deep learning-based acceleration technique. In this study, ACS employs a randomized undersampling strategy, resulting in 9 levels of undersampling in total. The associated acceleration factor varies between 2 and 4.

In this study, ACS-enabled images were compared to routine clinical images using quantitative and qualitative

Table 3 Quantitative parameter values across each region

Body regions	SNR		CNR		EC		EME	
	Non-ACS	ACS	Non-ACS	ACS	Non-ACS	ACS	Non-ACS	ACS
Brain	38.91 ± 1.29	41.13 ± 1.50	21.23 ± 5.21	22.67 ± 5.71	14.31 ± 5.72	22.63 ± 5.43	8.57 ± 1.43	11.42 ± 2.15
Spine	44.20 ± 4.26	46.35 ± 4.90	28.12 ± 5.67	29.78 ± 5.72	51.67 ± 1.48	73.58 ± 3.32	9.19 ± 0.30	9.56 ± 1.28
Liver	42.16 ± 1.31	44.89 ± 2.25	19.89 ± 3.61	21.98 ± 4.28	10.11 ± 1.85	16.68 ± 1.78	12.00 ± 0.39	15.65 ± 1.32
Kidney	42.43 ± 1.69	44.78 ± 2.12	25.72 ± 1.98	29.30 ± 3.68	60.85 ± 7.98	68.78 ± 5.11	7.94 ± 1.36	19.13 ± 3.77
Knee	38.34 ± 3.56	42.40 ± 2.51	24.70 ± 1.94	28.20 ± 2.54	20.95 ± 5.75	25.51 ± 5.54	9.13 ± 1.14	11.85 ± 1.43

SNR Signal to noise ratio, *CNR* Contrast to noise ratio, *EC* Edge content, *EME* Enhancement measure

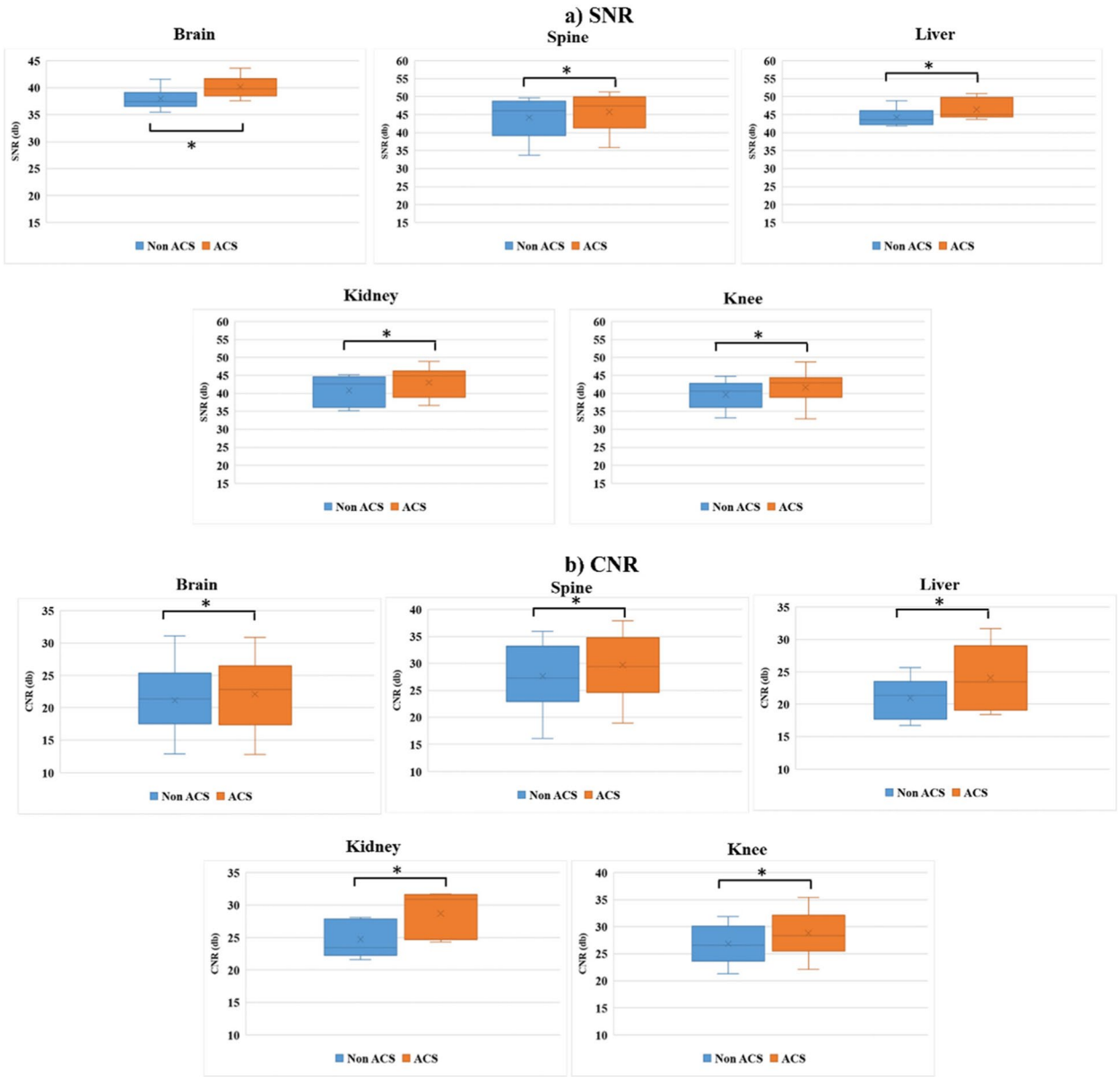

Fig. 5 Box Plots for SNR and CNR across all body regions for ACS vs. non-ACS MR images. There was a statistically significant improvement ($p < 0.05$) in the SNR and CNR of ACS images across all body regions, as denoted by the symbol '*'. SNR = Signal to noise ratio, CNR = Contrast to noise ratio

analysis. Artefacts in images, sharpness of tissue edges, overall image quality, and diagnostic efficiency of images were among the subjective image quality assessment parameters. SNR, CNR, EC and EME were measured for quantitative evaluation. Three radiologists evaluated the non-ACS and ACS images independently using proposed qualitative scoring criteria. Radiologists examined and assessed a total of 532 images. All images were randomized before being presented to the radiologists for evaluation. This randomization process ensures that the sequence in which the images are viewed does not introduce any systematic bias.

The results of the current study showed that the diagnostic quality of images acquired with ACS was on equivalent with or superior to images acquired without ACS based on the radiologists scores. The statistical test has been performed using two ways, first test was performed separately for each anatomical region, showing no significant difference ($p > 0.05$) in qualitative scores between non-ACS and ACS across each region, and second test was performed on all 532 images for overall comparison between the two sets of images, However, no significant difference was found between them. There was a good inter-observer agreement among all

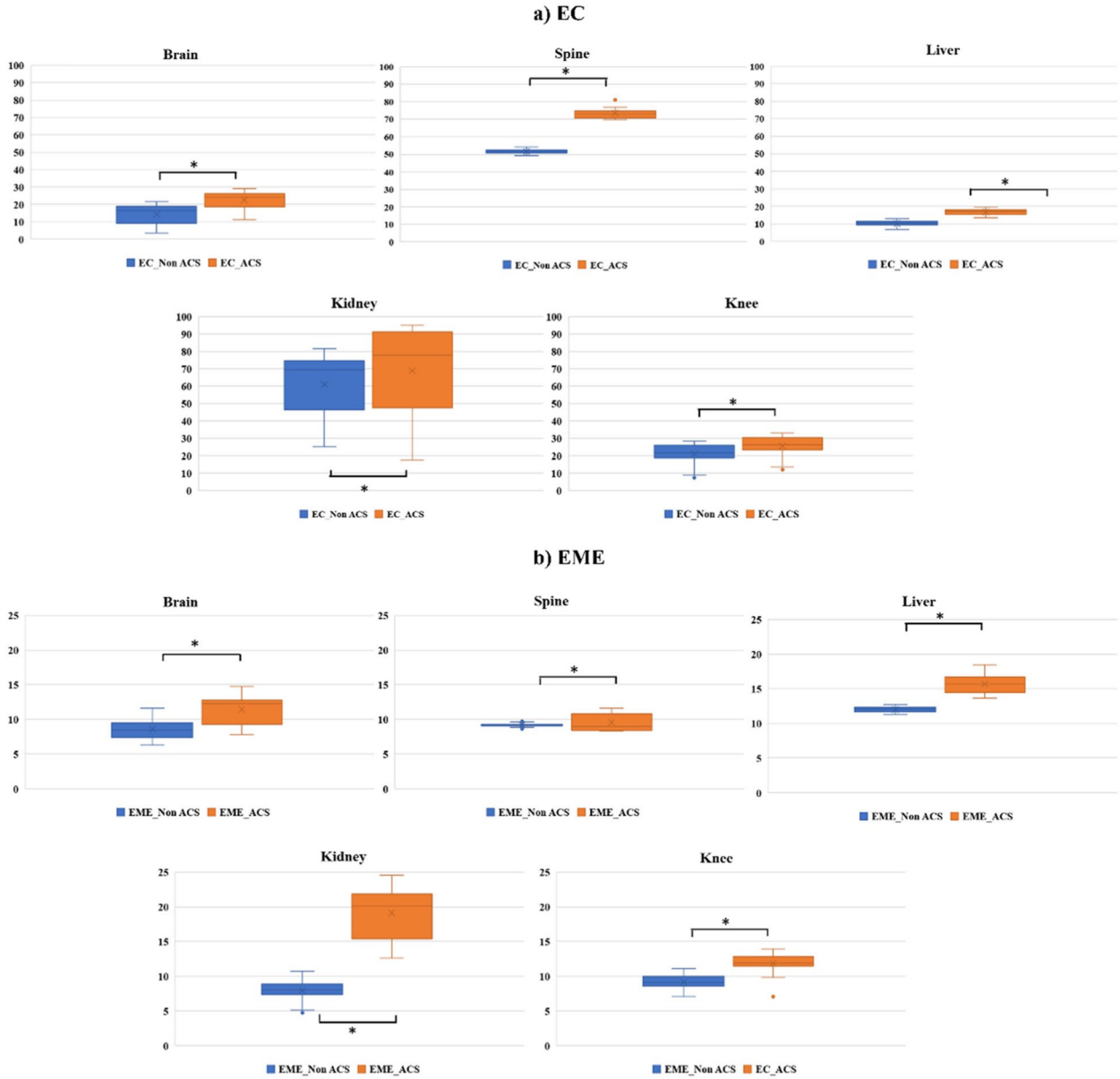

Fig. 6 Box Plots for EC and CME across all body regions for ACS vs. non-ACS MR images. There was a statistically significant improvement ($p < 0.05$) in EC and EME of ACS images across all body regions, as denoted by the symbol '*'. SNR = Signal to noise ratio, CNR = Contrast to noise ratio

radiologists (~0.70). The ACS sequence significantly reduces (by more than 50%) the scan time for all body regions and enables faster scans, which is also consistent with the recent review article [26]. Despite the subjective image quality of ACS being comparable to non-ACS (shown in Fig. 3), the clear advantage of ACS lies in its ability to reduce scanning time. This reduction in scan time not only improves patient comfort but also enhances clinical workflow by increasing patient throughput and reducing waiting times, which is critical in busy clinical environments.

In contrast to conventional non-ACS MR imaging, ACS was designed to mitigate the aliasing and noise typically seen in undersampled datasets. However, it is important to note that ACS may introduce its own set of artifacts. The rapid acquisition times provided by ACS not only enhance image quality but also help to mitigate motion artifacts, which are often a challenge in conventional imaging techniques. The concept of "motion freeze" achieved through fast scanning allows for clearer images by minimizing motion-related blurring, thus providing more reliable diagnostic information.

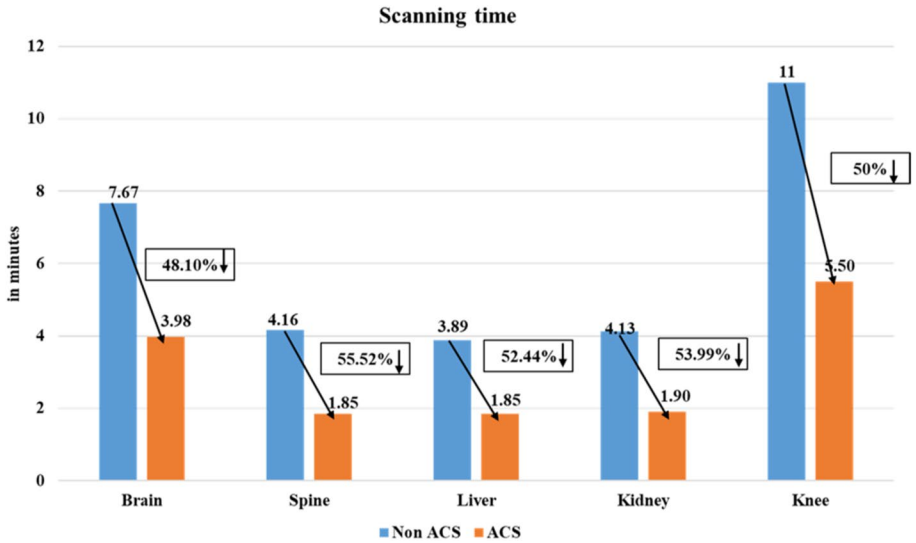

Fig. 7 Total scanning time across all sequences for different body regions with percentage difference in scanning time between ACS and non-ACS in minutes

During our qualitative evaluation, subtle instances of over-smoothing were observed in ACS-reconstructed images, particularly in regions with fine anatomical structures. This was likely a result of the network prioritizing artifact suppression, occasionally at the cost of spatial resolution. Additionally, ACS algorithms may introduce minor checkerboard patterns due to the upsampling process. These artifacts were absent in conventional MR imaging but were generally rare and did not affect the diagnostic interpretation of the images.

SNR and CNR are the parameters that have traditionally been used to demonstrate image quality with a reasonable amount of time for its acquisition. There is a trade-off between these parameters, and the SNR/CNR must be improved while the scan time is shortened [36]. In addition, EC and EME were used as quantitative parameters to measure the degree of contrast enhancement in both images. The denoising step ensures that the EC calculation reflects the true edges of the anatomical structures rather than noise artifacts [9, 30, 31]. Radiologists assisted in performing ROI marking for brain, spine, liver, kidney, and knee imaging. ROIs have been defined at the locations that are clinically significant to detect probable specific pathological abnormalities.

ACS uses deep learning approach to predict and recover lost data, resulting in enhanced edge definition and finer transitions between tissues. Conventional MR imaging uses fully sampled k-space data and standard reconstruction techniques. These methods generate high-quality images but may take longer to acquire and be more prone to motion artifacts, which reduce edge quality. The study indicates that the reconstruction times for ACS and non-ACS protocols are almost identical, with non-ACS being marginally faster by 1–2 s. This minor difference suggests that other factors, particularly those related to image quality and diagnostic accuracy, should be the main considerations in protocol selection.

In this study, it was found that the ACS technique achieves a significantly higher quantitative parameter values compared to non-ACS or routine MR images, which is also consistent with the literature [13, 22, 37]. The ACS technique has demonstrated higher image quality scores due to its advanced reconstruction algorithms, which efficiently reduce noise and enhance resolution. ACS network employs deep learning-based regularization, which aids in mitigating the effects of undersampling by effectively learning representations from prior data. This leads to superior noise management, improved edge preservation, and better contrast enhancement compared to traditional techniques, which lack such data-driven regularization. The adversarial component further encourages the generator to produce images that appear more realistic, thereby enhancing textural features and boundary sharpness, which ultimately contribute to higher metrics across SNR, CNR, EC, and EME.

In this study, not every subject underwent all five types of MR imaging. The dataset is designed to represent various clinical applications, so different subjects contributed to different anatomical regions, reflecting the diversity of real-world clinical imaging scenarios. CS and AI algorithms offer significant advantages in MR imaging, they can also introduce or fail to correct specific artifacts that impact overall image quality and

diagnostic accuracy. Common artifacts associated with these techniques include over-smoothing, ring artifacts, and checkerboard patterns.

The high computational demands of ACS require substantial processing power and memory, which can limit their practical implementation in clinical environments. In earlier studies, parallel computing technology was utilized to manage computationally intensive tasks, yielding impressive outcomes. Zhai et al. [38] implemented a real-time automatic segmentation system for cerebral aneurysms on a Zynq system-on-chip, subsequently creating an efficient hardware architecture based on the lattice Boltzmann method [39]. Esfahani et al. [40] developed an enhanced version of HemeLB, which served as the primary computational engine of their pipeline to facilitate real-time visualization and guidance for cerebral blood flow image acquisition. Additionally, Zhai et al. [41] designed and assessed a variant of HemeLB across multiple heterogeneous system-on-chip platforms, achieving real-time visualization of simulation results and significantly enhancing algorithm performance through acceleration.

Pre-processing steps and additional regularization techniques play a crucial role to enhance the robustness of ACS methods and address issues such as artifacts and variability. Regularization techniques are essential for preventing overfitting and enhancing the model's ability to generalize across different data conditions. In previous studies, a novel neural network (Res-PAC-UNet) with a fixed-width residual UNet backbone and Pyramid Atrous Convolutions was used for precise liver CT segmentation with low disk utilization [42]. Machine learning models have redirected drugs to the blood–brain barrier using advanced fingerprint amalgamation and data balancing techniques [15], while the Pyramid Scene Parsing (PSP) module in tuned neural networks enabled real-time liver segmentation without sacrificing accuracy [43]. Additionally, cross-modality image registration techniques have improved consistency and alignment across different imaging modalities [44].

Limitations

The lack of a universal standard for assessing the quality of ACS MR images is a major challenge in this field. There is a pressing need for a consensus framework or standardized set of metrics to evaluate ACS images quality. Such a framework would enable more consistent evaluations and comparisons across studies, thereby advancing the field and enhancing the clinical applicability of ACS methods. ACS method may exhibit performance variability when applied across different types of MRI machines, imaging protocols, or imaging conditions. Future research should focus on developing algorithms that can generalize across diverse MRI environments and standardizing imaging protocols where possible to enhance the consistency and reliability of ACS methods. In this study, data was collected from one institution and a small cohort, which could have an impact on the results. A large cohort and multicentre study can provide stronger evidence for larger clinical applications. The clinical significance of the study is limited by the lack of diseased subjects, which restricts interpretation of the results in a clinical context. Although this study evaluates image quality, it may not fully address specific artifacts introduced or inadequately corrected by ACS methods. Despite these limitations, the use of ACS technique in diagnostic imaging is a rapidly evolving field with the potential to significantly benefit patients and healthcare providers in the future.

Conclusion

In this study, both qualitative and quantitative analyses demonstrated that images acquired with ACS were superior to those obtained without ACS. The findings indicate that ACS not only preserves high image quality but also significantly reduces scan time. This improvement in both speed and image quality underscores the potential of ACS to enhance clinical workflows and patient outcomes in routine MRI practice. This makes ACS a valuable option in routine clinical practice, where patient throughput and comfort is essential.

Abbreviations

ACS	Artificial Intelligence assisted compressed sensing
CNN	Convolution neural network
CNR	Contrast-to-noise ratio
EC	Edge content
EME	Enhancement measure
FSE	Fast spin echo
MRI	Magnetic resonance imaging
SNR	Signal-to-noise ratio

Acknowledgements

Authors would like to acknowledge support staffs of Sprint Diagnostics, Jubilee Hills, Hyderabad, India for their valuable assistance during the data acquisition process and United Imaging healthcare.

Authors' contributions

Conceptualization: D.S., D.K. and A.G.; methodology: D.S., D.K., A.G., A.K.; formal analysis and investigation: D.S., A.G.; writing-original draft preparation: D.S.; resources: D.K., A.K., K.A., A.K., L.H.; supervision: D.K., A.K., K.A., A.K., L.H.

Funding

This research did not receive any specific grant from funding agencies in the public, commercial, or not-for-profit sectors.

Data availability

The datasets generated during and/or analyzed during the current study are not publicly available but are available from the corresponding author on reasonable request.

Declarations

Ethics approval and consent to participate

The study was approved by the IRB (ref: S-2022001) of Sprint Diagnostics, Hyderabad. All methods were carried out in accordance with relevant guidelines and regulations or the Declaration of Helsinki. All informed consent was obtained from the subjects and/or their legal guardian(s).

Consent for publication

Not applicable.

Competing interests

The authors declare no competing interests.

Author details

[1]Department of Radiology, Sprint Diagnostics, Jubilee Hills, Hyderabad, India. [2]Department of Radiology, SSB Hospital, Faridabad, India. [3]Department of Radiology, City Imaging & Clinical Labs, Delhi, India. [4]Central Research Institute, United Imaging Healthcare, Shanghai, China. [5]Central Research Institute, United Imaging Healthcare, Houston, USA.

Received: 15 August 2024 Accepted: 11 October 2024
Published online: 21 October 2024

References

1. Rao R, Venkatesan R, Geethanath S. Role of MRI in medical diagnostics. Resonance. 2015;20:1003–11. https://doi.org/10.1007/s12045-015-0268-2.
2. Bitar R, Leung G, Perng R, et al. MR pulse sequences: what every radiologist wants to know but is afraid to ask. Radiographics. 2006;26(2):513–37. https://doi.org/10.1148/rg.262055063.
3. Kozak BM, Jaimes C, Kirsch J, Gee MS. MRI techniques to decrease imaging times in children. Radiographics. 2020;40(2):485–502. https://doi.org/10.1148/rg.2020190112.
4. Xiang L, Chen Y, Chang W, et al. Ultra-fast T2-weighted MR reconstruction using complementary T1-weighted information. Med Image Comput Comput Assist Interv. 2018;11070:215–23. https://doi.org/10.1007%2F978-3-030-00928-1_25.
5. van Sambeek JR, Joustra PE, Das SF, et al. Reducing MRI access times by tackling the appointment-scheduling strategy. BMJ Qual Saf. 2011;20(12):1075–80. https://doi.org/10.1136/bmjqs.2010.049643.
6. Garwood ER, Recht MP, White LM. Advanced imaging techniques in the knee: benefits and limitations of new rapid acquisition strategies for routine knee MRI. AJR Am J Roentgenol. 2017;209:552–60. https://doi.org/10.2214/ajr.17.18228.
7. Magnotta VA, Friedman L, FIRST BIRN. Measurement of signal-to-noise and contrast-to-noise in the fBIRN multicenter imaging study. J Digit Imaging. 2006;19(2):140–7. https://doi.org/10.1007%2Fs10278-006-0264-x.
8. Akila K, Jayashree L, Vasuki A. Mammographic image enhancement using indirect contrast enhancement techniques–a comparative study. Procedia Comput Sci. 2015;47:255–61. https://doi.org/10.1016/j.procs.2015.03.205.
9. Gandhamal A, Talbar S, Gajre S, Hani AF, Kumar D. Local gray level S-curve transformation - a generalized contrast enhancement technique for medical images. Comput Biol Med. 2017;83:120–33. https://doi.org/10.1016/j.compbiomed.2017.03.001.
10. Wang S, Su Z, Ying L, et al. Accelerating magnetic resonance imaging via deep learning. In: 2016 IEEE 13th International Symposium on Biomedical Imaging (ISBI). Prague: IEEE. 2016;514–7. https://doi.org/10.1109/ISBI.2016.7493320.
11. Shrividya G, Bharathi SH. Application of compressed sensing on magnetic resonance imaging: a brief survey. In: 2016 IEEE International Conference on Recent Trends in Electronics, Information & Communication Technology (RTEICT). Bangalore: IEEE. 2016;2037–41. https://doi.org/10.1109/RTEICT.2016.7808197.
12. Huang F, Lin W, Li Y. Partial fourier reconstruction through data fitting and convolution in k-space. Magn Reson Med. 2009;62(5):1261–9. https://doi.org/10.1002/mrm.22128.
13. Sheng RF, Zheng LY, Jin KP, et al. Single-breath-hold T2WI liver MRI with deep learning-based reconstruction: a clinical feasibility study in comparison to conventional multi-breath-hold T2WI liver MRI. Magn Reson Imaging. 2021;81:75–81. https://doi.org/10.1016/j.mri.2021.06.014.
14. Chandrasekar V, Ansari MY, Singh AV, et al. Investigating the use of machine learning models to understand the drugs permeability across placenta. IEEE Access. 2023;11:52726–39. https://doi.org/10.1109/ACCESS.2023.3272987.
15. Ansari MY, Chandrasekar V, Singh AV, et al. Re-routing drugs to blood brain barrier: a comprehensive analysis of machine learning approaches with fingerprint amalgamation and data balancing. IEEE Access. 2023;11:9890–906. https://doi.org/10.1109/ACCESS.2022.3233110.
16. Ansari MY, Qaraqe M, Righetti R, et al. Unveiling the future of breast cancer assessment: a critical review on generative adversarial networks in elastography ultrasound. Front Oncol. 2023;6(13):1282536. https://doi.org/10.3389/fonc.2023.1282536.
17. Ansari MY, Mangalote IAC, Meher PK. Advancements in deep learning for B-mode ultrasound segmentation: a comprehensive review. IEEE Trans Emerg Top Comput Intell. 2024;8(3):2126–49. https://doi.org/10.1109/TETCI.2024.3377676.
18. Ansari MY, Mangalote IAC, Masri D, et al. Neural network-based fast liver ultrasound image segmentation. In: 2023 IEEE International Joint Conference on Neural Networks (IJCNN). Gold Coast: IEEE. 2023;1–8. https://doi.org/10.1109/IJCNN54540.2023.10191085.
19. Ansari MY, Mohanty S, Mathew SJ, et al. Towards developing a lightweight neural network for liver CT segmentation. In: Su R, Zhang Y, Liu H, F Frangi A. (eds) Medical imaging and computer-aided diagnosis. MICAD 2022. Lecture Notes in Electrical Engineering. Singapore: Springer. 2023;810:27–35. https://doi.org/10.1007/978-981-16-6775-6_3.
20. Ansari MY, Qaraqe M, Charafeddine F, et al. Estimating age and gender from electrocardiogram signals: a comprehensive review of the past decade. Artif Intell Med. 2023;146:102690. https://doi.org/10.1016/j.artmed.2023.102690.
21. Ansari MY, Qaraqe M, Righetti R, et al. Enhancing ECG-based heart age: impact of acquisition parameters and generalization strategies for varying signal morphologies and corruptions. Front Cardiovasc Med. 2024;11:1424585. https://doi.org/10.3389/fcvm.2024.1424585.
22. Ghodrati V, Shao J, Bydder M, et al. MR image reconstruction using deep learning: evaluation of network structure and loss functions. Quant Imaging Med Surg. 2019;9(9):1516–27. https://doi.org/10.21037%2Fqims.2019.08.10.
23. Li H, Hu C, Yang Y, et al. Single-breath-hold T2WI MRI with artificial intelligence-assisted technique in liver imaging: as compared with conventional respiratory-triggered T2WI. Magn Reson Imaging. 2022;93:175–218. https://doi.org/10.1016/j.mri.2022.08.012.
24. Wang Q, Zhao W, Xing X, et al. Feasibility of AI-assisted compressed sensing protocols in knee MR imaging: a prospective multi-reader study. Eur Radiol. 2023;33(12):8585–96. https://doi.org/10.1007/s00330-023-09823-6.
25. Zhao Y, Peng C, Wang S, Liang X, Meng X. The feasibility investigation of AI -assisted compressed sensing in kidney MR imaging: an ultra-fast T2WI imaging technology. BMC Med Imaging. 2022;22(1):119–27. https://doi.org/10.1186/s12880-022-00842-1.
26. Priyanka KR, Nayak SS, Chandran M, et al. Impact of artificial intelligence assisted compressed sensing technique on scan time and image quality in musculoskeletal MRI - a systematic review. Radiography (Lond). 2024;S1078–8174(24):00212–8. https://doi.org/10.1016/j.radi.2024.08.012.
27. Zhai R, Huang X, Zhao Y, et al. Intelligent incorporation of AI with model constraints for MRI acceleration. In: Proceedings of the 29th Annual Meeting of ISMRM [Virtual]. 2021. https://archive.ismrm.org/2021/1760.html.
28. Quan TM, Nguyen-Duc T, Jeong WK. Compressed sensing MRI reconstruction using a generative adversarial network with a cyclic loss. IEEE Trans Med Imaging. 2018;37:1488–97. https://doi.org/10.1109/TMI.2018.2820120.
29. Yang G, Yu S, Dong H, et al. DAGAN: deep de-aliasing generative adversarial networks for fast compressed sensing MRI reconstruction. IEEE Trans Med Imaging. 2018;37:1310–21. https://doi.org/10.1109/TMI.2017.2785879.
30. Gupta S, Porwal R. Appropriate contrast enhancement measures for brain and breast cancer images. Int J Biomed Imaging. 2016;4710842. https://doi.org/10.1155/2016/4710842.

31. Again SS, Panetta, Grigoryan AM. Transform-based image enhancement algorithms with performance measure. IEEE Trans Image Process. 2001;10(3):367–382. https://doi.org/10.1109/83.908502.
32. Andre JB, Bresnahan BW, Mossa-Basha M, et al. Toward quantifying the prevalence, severity, and cost associated with patient motion during clinical MR examinations. J Am College Radiol. 2015;12(7):689–95. https://doi.org/10.1016/j.jacr.2015.03.007.
33. Johnson PM, Recht MP, Knoll F. Improving the speed of MRI with artificial intelligence. Semin Musculoskelet Radiol. 2020;24:12–20. https://doi.org/10.1055/s-0039-3400265.
34. Hammernik K, Klatzer T, Kobler E, et al. Learning a variational network for reconstruction of accelerated MRI data. Magn Reson Med. 2018;79:3055–71. https://doi.org/10.1002/mrm.26977.
35. Knoll F, Hammernik K, Kobler E, et al. Assessment of the generalization of learned image reconstruction and the potential for transfer learning. Magn Reson Med. 2019;81:116–212. https://doi.org/10.1002/mrm.27355.
36. Wu HH, Nishimura DG. 3D magnetization-prepared imaging using a stack-of-rings trajectory. Magn Reson Med. 2010;63(5):1210–8 https://doi.org/10.1002%2Fmrm.22288.
37. Sui H, Gong Y, Liu L, et al. Comparison of artificial intelligence-assisted compressed sensing (ACS) and routine two-dimensional sequences on lumbar spine imaging. J Pain Res. 2023;16:257–67. https://doi.org/10.2147/jpr.s388219.
38. Zhai X, Eslami M, Hussein ES, et al. Real-time automated image segmentation technique for cerebral aneurysm on reconfigurable system-on-chip. J Comput Sci. 2018;27:35–45. https://doi.org/10.1016/j.jocs.2018.05.002.
39. Zhai X, Amira A, Bensaali F, et al. Zynq SoC based acceleration of the lattice boltzmann method. Concurrency Computation: Pract Experience. 2019;31(17):e5184. https://doi.org/10.1002/cpe.5184.
40. Esfahani SS, Zhai X, Chen M, et al. Lattice-Boltzmann interactive blood flow simulation pipeline. Int J Comput Assist Radiol Surg. 2020;15(4):629–39. https://doi.org/10.1007/s11548-020-02120-3.
41. Zhai X, Chen M, Esfahani SS, et al. Heterogeneous system-on-chip-based Lattice-Boltzmann visual simulation system. IEEE Syst J. 2019;14(2):1592–601. https://doi.org/10.1109/JSYST.2019.2952459.
42. Ansari MY, Yang Y, Balakrishnan S, et al. A lightweight neural network with multiscale feature enhancement for liver CT segmentation. Sci Rep. 2022;12:14153. https://doi.org/10.1038/s41598-022-16828-6.
43. Ansari MY, Yang Y, Meher PK, et al. Dense-PSP-UNet: a neural network for fast inference liver ultrasound segmentation. Comput Biol Med. 2023;153:106478. https://doi.org/10.1016/j.compbiomed.2022.106478.
44. Mohanty S, Dakua SP. Toward computing cross-modality symmetric non-rigid medical image registration. IEEE Access. 2022;10:24528–39. https://doi.org/10.1109/ACCESS.2022.3154771.

Publisher's Note